AIAA SciTech Forum
8–12 January 2018, Kissimmee, Florida
2018 AIAA Aerospace Sciences Meeting

10.2514/6.2018-0829

Comparison of h- and p-Derived Output-Based Error Estimates for Directing Anisotropic Adaptive Mesh Refinement in Three-Dimensional Inviscid Flows

Christopher N. Ngigi*, Lucie Freret† and Clinton P. T. Groth‡
University of Toronto Institute for Aerospace Studies,
4925 Dufferin Street, Toronto, Ontario, M3H 5T6, Canada

The use of adjoint-based error estimation in conjunction with a highly parallel and scalable, anisotropic, block-based, adaptive mesh refinement (AMR) technique is considered for the more efficient prediction of three-dimensional compressible flows. In particular, a comparison is made between the computational performances of output-based error estimates, derived via two approaches, namely one based on mesh (or h) refinement and the other based on order (or p) refinement, for directing the mesh refinement in anisotropic AMR scheme. The AMR scheme allows enhancement of local mesh resolution, with preference given to directions as dictated by the flow solution. The proposed adjoint-based error estimation technique provides *a posteriori* estimates of the error for an engineering functional of interest in terms of estimates of the local solution error following from the solution residual. The estimated error in the solution residual is obtained either via direct refinement of the mesh in the preferred directions (here referred to as the h-derived error indicator) or by using a higher-order spatial operator with anisotropic feature detection based on the anisotropic smoothness indicator of an appropriate solution quantity (here referred to as the p-derived error indicator). Both approaches are considered here. Additionally, two formulations of the adjoint-based error indicator are examined for directing the output-based AMR. The first is the so-called computable correction (CC), where the residual error is weighted by the corresponding adjoint solution for the functional of interest, and the second is the so-called error in the computable correction (ECC), which is comprised of a linear combination of the residual error weighted with the adjoint solution and the adjoint residual weighted with the primal solution. The resulting output error indicator is used to direct the mesh refinement, with regions of the solution domain contributing most significantly to the functional error being selected for local enrichment of the mesh. In this way, the computed accuracy of the functional is increased while potentially greatly reducing the associated computational cost of performing the simulation. For the cases of interest, both low- and high-order upwind finite-volume spatial discretization schemes are applied in conjunction with the block-based AMR scheme to the solution of the partial differential equations governing steady-state inviscid compressible flows. The potential benefits of the proposed anisotropic block-based AMR with adjoint-based error estimation are demonstrated for a range of compressible inviscid flow problems of varying complexity. Comparisons of solution accuracy and relative computational costs for results obtained using both h- and p-derived error estimates of the solution residual are examined and discussed.

I. Introduction and Motivation

One approach to reducing computational costs of predicting complex physical flows having disparate spatial scales is provided by adaptive mesh refinement (AMR) techniques.[1–8] These techniques make use of increased mesh resolution only in selected areas of the computational domain requiring higher spatial

*Ph. D. Candidate, chris.ngigi@mail.utoronto.ca
†Post-Doctoral Fellow
‡Professor, AIAA Senior Member.

resolution, thereby significantly reducing the overall mesh size for problems with multiple scales while still providing the desired solution accuracy. The parallel block-based AMR techniques proposed by Groth and co-workers[9–15] are of interest here and have been shown to be very effective for solving physically complex flows on multi-block body-fitted hexahedral meshes using distributed memory parallel computers. The isotropic block-based AMR, as originally proposed by Gao and Groth,[9,12,13] makes use of an octree data structure wherein each block flagged for refinement is refined equally in all directions. The isotropic block-based AMR methods have been applied quite extensively to combustion problems by Groth and co-workers. For example, Northrup and Groth[10,16,17] used the isotropic block-based AMR for simulation of laminar steady and unsteady premixed and non-premixed flames. Gao and Groth[9,12,13,18–20] and Jha[21] applied isotropic block-based AMR to turbulent diffusion flames. Ivan *et al.*[22,23] and Susanto *et al.*[24] have also used block-based AMR for magnetohydrodynamic simulations. An anisotropic version of the block-based AMR based on a binary-tree data structure was more recently proposed by Zhang and Groth[25] so as to increase further the computational savings. When applied to convection-diffusion and the inviscid flow equations, significant mesh savings were found. Williamschen and Groth[26] extended this anisotropic block-based AMR to 3D simulations of inviscid flows governed by the Euler equations. They used a uniform block approach where the ghost cells for a block had the same refinement level as the block itself. More recently, an anisotropic block-based approach making use of heterogeneous non-uniform blocks was proposed by Freret and Groth.[15] The latter has several advantages making it more efficient and better suited for high-order spatial discretizations. The extension of the anisotropic AMR approach for use with the high-order central essentially non-oscillatory (CENO) finite-volume scheme is considered in the recent study by Freret *et al.*[27]

In many of the aforementioned studies, physics- and/or gradient-based strategies were used to identify regions for mesh refinement by monitoring solution quantity changes over spatial ranges. These approaches are easily implementable and work well for many of the problems studied. However, the gradient-based techniques have been shown to have limitations,[15,28] some of which include the potential over-refinement of regions in the vicinity of shocks and discontinuities, the potential lack of convergence for a measured solution error-norm despite continued mesh refinement, and the challenge of correctly identifying refinement regions where smooth solutions exist. To avoid the shortcomings of physics- and/or gradient-based refinement strategies mentioned above, the use of adjoint-based error estimation is considered here for directing the mesh adaptation. In particular, the application of adjoint-based error estimation as proposed by a number of previous researchers[29–39] is examined for directing mesh refinement in the anisotropic block-based AMR approach of Freret and Groth[15] as well as Freret *et al.*[27] The adjoint-based error estimation is used to evaluate the sensitivity of pre-defined engineering quantities or functionals of interest to corresponding local estimates of the solution error. This output-based error estimate is calculated here via two approaches: one based on mesh (or h) refinement and the other based on order (or p) refinement and these estimates are then used to direct the mesh adaptation. A primary benefit of the proposed approach is the refinement of relevant regions within the computational domain that have the highest sensitivity to errors in the functional of interest, leading to a more rapid convergence of the predicted value for the functional as the mesh is refined.

II. Scope of Present Study

In the present study, a second-order limited upwind finite-volume spatial discretization scheme is used along with the anisotropic block-based AMR scheme of Freret and Groth[15] and Freret *et al.*[27] for the solution of compressible form of Euler equations on three-dimensional multi-block body-fitted meshes consisting of hexahedral computational cells. High-order residual evaluation associated with p-refinement is carried out using the high-order central essentially non-oscillatory (CENO) finite-volume scheme of Ivan and Groth[40] that was recently extended for use with the anisotropic block-based AMR scheme. The low- and high-order finite-volume schemes and anisotropic AMR method are first discussed and then a description of the proposed adjoint-based error estimation strategy and output-driven refinement procedure are given. Both h- and p-based strategies for evaluating the functional error and refinement criteria are discussed. This is followed by a discussion of numerical results for a range of compressible inviscid flow problems of varying complexity. The performance and suitability of the proposed output-based error estimation and AMR strategy are demonstrated by comparing the results obtained using both the output-based anisotropic refinement and previous gradient-based strategies, as well as to results obtained using uniform refinement. The reduction in the estimated error in the functional is examined and compared as are the relative computational costs of the various strategies.

III. Finite-Volume Scheme and Anisotropic Block-Based AMR

III.A. Governing Equations

The proposed anisotropic AMR scheme is applied to the solution of three-dimensional Euler equations governing inviscid compressible flows of a polytropic gas. These equations can be expressed in conservative form as

$$\frac{\partial \mathbf{U}}{\partial t} + \nabla \cdot \vec{\mathbf{F}} = \mathbf{0}, \tag{1}$$

where $\mathbf{U}$ is the vector of conserved variables reflecting conservation of mass, momentum, and energy for the fluid and $\vec{\mathbf{F}}$ is the flux dyad. For a three dimensional Cartesian coordinate system, the Euler equations can be written as

$$\frac{\partial \mathbf{U}}{\partial t} + \frac{\partial \mathbf{F}}{\partial x} + \frac{\partial \mathbf{G}}{\partial y} + \frac{\partial \mathbf{H}}{\partial z} = 0, \tag{2}$$

where column vectors $\mathbf{F}$, $\mathbf{G}$, $\mathbf{H}$, are the inviscid flux vectors associated with the solution flux in the x, y, and z directions, respectively, such that $\vec{\mathbf{F}} = [\mathbf{F}, \mathbf{G}, \mathbf{H}]$. The solution and inviscid flux vectors are given by

$$\mathbf{U} = \begin{bmatrix} \rho \\ \rho u \\ \rho v \\ \rho w \\ e \end{bmatrix}, \mathbf{F} = \begin{bmatrix} \rho u \\ \rho u^2 + p \\ \rho uv \\ \rho uw \\ \rho uh \end{bmatrix}, \mathbf{G} = \begin{bmatrix} \rho v \\ \rho vu \\ \rho v^2 + p \\ \rho vw \\ \rho vh \end{bmatrix}, \mathbf{H} = \begin{bmatrix} \rho w \\ \rho wu \\ \rho wv \\ \rho w^2 + p \\ \rho wh \end{bmatrix}. \tag{3}$$

where ρ is the density, u, v, w are x, y, z velocity components, respectively, $e = p/(\rho(\gamma - 1)) + u^2/2$ is the specific total energy and $h = e + p$ is the specific enthalpy. The ideal gas equation $p = \rho RT$ is used for closure of the system where T is the gas temperature and R is the ideal gas constant. The ratio of specific heats $\gamma = C_p/C_v$ is assumed to be constant.

III.B. Limited Second-Order Finite-Volume Scheme and Semi-Discrete Form

Following application of a standard finite-volume method to a hexahedral computational cell or element, (i, j, k), of a structured three-dimensional grid, Eq. (1) can be re-expressed in semi-discrete form as

$$\frac{\mathrm{d}\mathbf{U}_{i,j,k}}{\mathrm{d}t} = -\mathbf{R}_{i,j,k}(\mathbf{U}) = -\frac{1}{V_{i,j,k}} \sum_{f=1}^{N_f} \left(\vec{\mathbf{F}}_f . \vec{\mathbf{n}}_f \Delta A_f \right)_{i,j,k}, \tag{4}$$

where $\mathbf{U}_{i,j,k}$ is the averaged conserved solution for cell (i, j, k), and $\mathbf{R}_{i,j,k}$ is the discrete residual calculated by summation of fluxes at the faces of cell (i, j, k). The variables $V_{i,j,k}$, $\vec{\mathbf{F}}_f$, $\vec{\mathbf{n}}_f$ and ΔA_f denote the cell volume, flux vector, outward pointing unit normal vector and the area of the cell face, f, respectively, and N_f is an integer value representing the number of faces for cell (i, j, k). The spatial discretization is accomplished herein by using a second-order cell-centered finite-volume scheme. Limited piecewise-linear least-squares reconstruction is used for calculating primitive flow variables at the cell faces. A Godunov-type flux function,[41] namely the so-called HLLE approximate Riemann solver based flux function proposed by Einfeldt,[42] is used for inviscid flux evaluation at the cell faces.

III.C. Inexact Newton's Method

For computing steady-state solutions to the Euler equations with $\mathrm{d}\mathbf{U}/\mathrm{d}t = 0$, Newton's method is applied to the solution of the coupled non-linear algebraic equations that results from the preceding spatial discretization procedure with $\mathbf{R}(\mathbf{U}) = 0$. The particular implementation applied here follows the algorithm developed by Northrup and Groth,[16] which is well adapted for computations on large multi-processor parallel clusters.

In this approach, an inexact Newton's method is used to solve the coupled system of non-linear algebraic equations given by

$$\frac{\mathrm{d}\mathbf{U}}{\mathrm{d}t} = -\mathbf{R}(\mathbf{U}) = 0. \tag{5}$$

These non-linear equations are linearized through the application of Newton's method to arrive at the following system of linear equations

$$\left[\frac{\partial \mathbf{R}}{\partial \mathbf{U}}\right] \Delta\mathbf{U}^{(n)} = \mathbf{J}\Delta\mathbf{U}^{(n)} = -\mathbf{R}(\mathbf{U}^{(n)}), \tag{6}$$

where $\mathbf{J} = \partial\mathbf{R}/\partial\mathbf{U}$ and $\mathbf{U}^{(n+1)} = \mathbf{U}^{(n)} + \Delta\mathbf{U}^{(n)}$. Thus, for a given initial estimate of the solution, $\mathbf{U}^{(n=0)}$, an improved approximation, $\mathbf{U}^{(n+1)}$, is obtained by solving the system of linear equations at each step, n, of Newton's method. The linear system of equations is solved iteratively until the solution residual is sufficiently small below a user-defined tolerance level.

Equation (6) is of the form

$$\mathbf{A}\mathbf{x} = \mathbf{b}, \tag{7}$$

and can be solved using an iterative linear solver. Such systems are typically very large, non-symmetric, and associated with sparse banded matrices. For large sparse systems, it is economical to use Krylov subspace methods. The Generalized Minimum Residual (GMRES) method, a class of Krylov subspace methods, initially developed by Saad and Schultz[43] is used here. GMRES is implemented here in a parallel fashion allowing use of parallel computer architectures having multiple processors using the Message Passing Interface (MPI) library of subroutines.[44,45] Refer to the paper by Northrup and Groth[16] for further details of the parallel Newton method used here.

The combined Newton method and limited-second-order finite-volume scheme are used here both for obtaining the solution to the flow problems of interest on the adapted meshes as well as in evaluating the solution residuals needed for computing the error indicators based on h-refinement of the mesh.

III.D. High-Order CENO Finite-Volume Scheme

The evaluation of error estimates for directing the anisotropic mesh refinement based on p refinement is also considered here and, for this, the evaluation of the solution residual to high-order (i.e., $p > 2$) is required. High-order evaluation of the solution residual is accomplished here by using the high-order CENO finite-volume and reconstruction scheme of Ivan and Groth[40] and Freret *et al.*[27] The CENO scheme is a hybrid approach that combines a high-order unlimited central scheme for fully resolved solution content with a low-order limited linear method for under-resolved/discontinuous content. To ensure monotonicity, switching from high- to low-order is controlled by a smoothness indicator. In contrast to other essential non-oscillatory (ENO) schemes[46,47] that require reconstruction on multiple stencils and present several additional computational complexities, the CENO scheme uses a single central stencil and thereby affords high-order accuracy at relatively lower computational cost. For the error estimation based on p-refinement considered here, a third-order evaluation, $p = 3$, is compared to the baseline second-order accurate, $p = 2$, residual.

III.D.1. Smoothness Indicator

The proposed CENO scheme of Ivan and Groth[40] preserves solution monotonicity in regions of non-smooth or discontinuous solutions by reverting back to a limited linear piecewise reconstruction. In order to detect regions where this should be done, a smoothness indicator is calculated for each variable within each cell as a post-analysis step after the unlimited high-order K-exact reconstruction has been performed. The smoothness indicator, S, is calculated based on a solution smoothness parameter, α, the number of unknowns (degrees of freedom, DOF), and the size of the stencil, SOS, used in the reconstruction. It is taken to have the form

$$\mathcal{S} = \frac{\alpha}{\max\left((1-\alpha), \epsilon\right)} \frac{(SOS - DOF)}{(DOF - 1)} \tag{8}$$

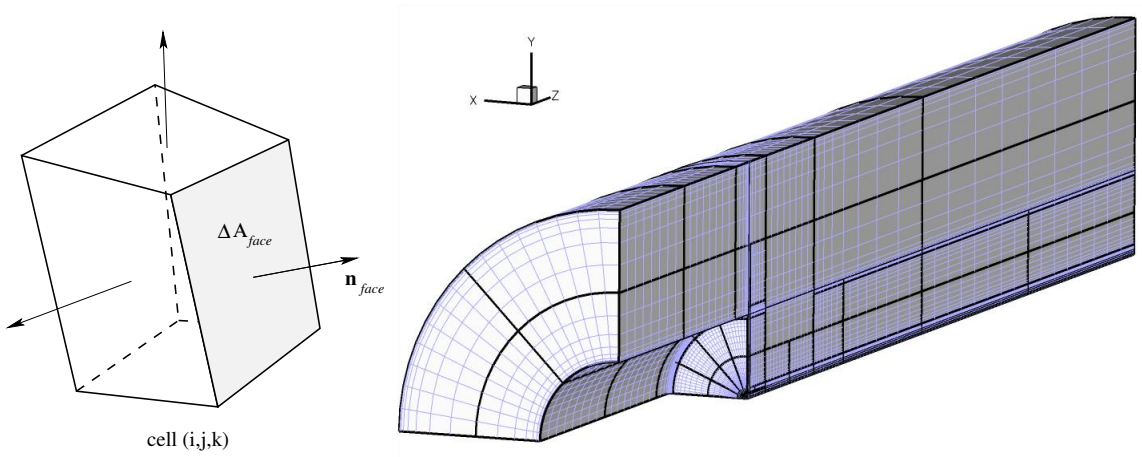

Figure 1: (a) Hexahedral cell at grid location i, j, k showing face normals. (b) Body-fitted adapted mesh after several refinements. Grid blocks are shown with bold lines.

where α is determined in terms of the K-exact reconstructed solution variable, $u^K_{i,j,k}$, in each cell (i, j, k) as follows

$$\alpha = 1 - \frac{\sum_{\gamma}\sum_{\delta}\sum_{\xi}\left(u^K_{\gamma,\delta,\xi}(\vec{r}_{\gamma,\delta,\xi}) - u^K_{i,j,k}(\vec{r}_{\gamma,\delta,\xi})\right)^2}{\sum_{\gamma}\sum_{\delta}\sum_{\xi}\left(u^K_{\gamma,\delta,\xi}(\vec{r}_{\gamma,\delta,\xi}) - \bar{u}_{i,j,k}\right)^2} \tag{9}$$

and where the ranges of the indices, γ, δ, and ξ, are taken to include all control volumes in the reconstruction stencil for cell (i, j, k), $\vec{r}_{\gamma,\delta,\xi}$ is the centroid of the cell (γ, δ, ξ), and the tolerance, ϵ, has been introduced in order to avoid division by zero. A suitable value for ϵ is 10^{-8}. It should be evident that the parameter α compares the values of the reconstructed solution at the centroids of neighbouring cells used in the solution reconstruction for cell (i, j, k). The range for α is $-\infty < \alpha \leq 1$ and it will approach unity as piecewise K-exact solution reconstruction within each cell yields a smooth and continuous representation of the solution between adjacent cells.

Note that Freret *et al.*[27] propose an anisotropic smoothness indicator to represent the smoothness of the solution in a particular logical or computational coordinate direction of the grid. The anisotropic smoothness indicator for a direction, γ, is evaluated using

$$\mathcal{S}_\gamma = \frac{\alpha_\gamma}{\max\left((1 - \alpha_\gamma), \epsilon\right)} \tag{10}$$

where α_γ is determined as follows

$$\alpha_\gamma = 1 - \frac{\sum_{\delta}\sum_{\xi}\left(u^K_{\gamma,\delta,\xi}(\vec{r}_{\gamma,\delta,\xi}) - u^K_{i,j,k}(\vec{r}_{\gamma,\delta,\xi})\right)^2}{\sum_{\delta}\sum_{\xi}\left(u^K_{\gamma,\delta,\xi}(\vec{r}_{\gamma,\delta,\xi}) - \bar{u}_{i,j,k}\right)^2} \tag{11}$$

The proposed smoothness indicator provides a measure of solution smoothness in the logical coordinate direction γ and can be used exploited in anisotropic refinement of the mesh.[27] This anisotropic smoothness indicator was utilized for determination of directional bias of the solution within the proposed output-based anisotropic AMR procedure based on p-refinement, as described in section IV.

III.E. Anisotropic Block-Based AMR

Anisotropic adaptive refinement of the three-dimensional multi-block body-fitted hexahedral meshes is accomplished here using the approach recently proposed and developed by Freret and Groth[15] and Freret *et*

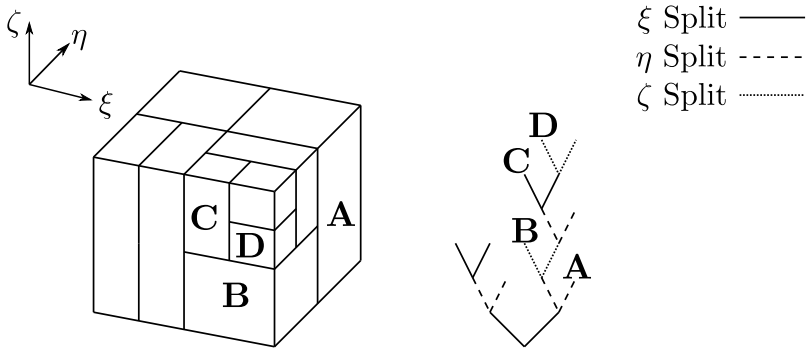

Figure 2: 3D binary tree and the corresponding blocks after several refinements

al.[27] In this approach, the hexahedral computational cells are grouped into blocks and mesh refinement is performed on a block basis, as opposed to individual cells. A schematic diagram of a hexahedral cell is shown in Figure 1(a) while an example of a body-fitted mesh generated using block-based AMR is illustrated in Figure 1(b). A hierarchical binary tree data structure is used to track the grid refinement and determine the neighbouring blocks as shown in Figure 2. Solution information from adjacent grid blocks is shared by utilizing layers of ghost cells in which the cell information for adjacent blocks is stored directly at the given level of refinement. This so-called non-uniform block approach for the ghost cell treatment eliminates the need for prolongation and restriction operators to fill ghost cells, also removes the need for flux corrections at block interfaces with grid resolution changes, and generally simplifies the parallel implementation of the AMR procedure, especially for the CENO high-order spatial discretization scheme. The resulting anisotropic AMR scheme also readily facilitates parallel implementation of the proposed finite-volume solution method[16,27] and provides the basis for performing the error-based mesh refinement considered herein.

IV. Adjoint-Based Error Estimation

Within the context of the proposed error-based AMR procedure, grid blocks of the computational mesh are flagged for refinement if they contribute significantly to the solution error while those grid blocks which have relatively minimal impact on the error are flagged for coarsening, thereby reducing unnecessary over-resolution of the mesh. Thresholds for the solution error are specified for both refinement and coarsening, providing control over the AMR procedure. In the adjoint-based approach considered herein, the mesh adaptation is based on an engineering functional or output and, for the purposes of the present study, the integrated pressure drag was used as the functional. The sensitivity of the pressure drag to local estimates of the error in the solution residual is then evaluated using a discrete adjoint formulation. Two formulations of the adjoint-based error indicator for the functional are examined herein. First is the so-called computable correction (CC), where the solution residual error is weighted by the corresponding adjoint (dual) solution for the functional of interest, and the second is the error in the computable correction (ECC), which is comprised of a linear combination of the residual error weighted with the adjoint solution, and the adjoint residual weighted with the primal solution as proposed by Venditti and Darmofal.[32,33,48] In the present work, evaluation of the adjoint-based error estimates are obtained based on both h- and p-refinement as described below. The resulting error estimates arising from these two methods and their performance in directing the AMR are also compared and contrasted to more commonly used gradient-based AMR strategies here. For the latter, the gradient of flow density was used to direct the AMR.

IV.A. Calculation of Fine-Space Error Indicator via h-Refinement

The h-refinement strategy adopted herein for the calculation of the fine-space error measure largely follows the dual-weighted residual approach that was originally advocated by Venditti and Darmofal.[32,33,48] Within the adjoint-based error estimation procedure, we are interested in the accurate evaluation of a scalar engineering functional, J, here taken to be the pressure drag for the application of interest. In general, J is a function of the 'primal' solution, $\mathbf{U}$, and can be expressed as $J = J(\mathbf{U})$. As a starting point, a converged steady-state primal solution, $\mathbf{U}_H$, on a 'coarse' grid, Ω_H, is obtained by solving the governing Euler equations

in semi-discrete form using the limited second-order finite-volume scheme described above for which the corresponding functional on the coarse space is evaluated as $J_H(\mathbf{U}_H)$ and where H here is a parameter that refers to the characteristic length associated with the coarse computational grid. Error estimates for directing mesh adaptation are then developed by considering an estimate for the value of a 'fine' space functional, $J_h(\mathbf{U}_h)$, based on primal solution, $\mathbf{U}_h$, evaluated on a corresponding 'fine' mesh, Ω_h, where h is indicative of fine mesh quantities. An estimate of the error in the functional, δJ, can be obtained without actually solving for the primal solution on the fine grid and can be expressed as in terms of the solution residual, $\mathbf{R}$, and written as

$$\begin{aligned}\delta J &= J_h(\mathbf{U}_h^H) - J_h(\mathbf{U}_h) \\ &\approx \underbrace{(\mathbf{\Psi}_h^H)^T \mathbf{R}_h(\mathbf{U}_h^H)}_{\text{computable correction}} + \underbrace{(\mathbf{R}_h^\Psi(\mathbf{\Psi}_h^H))^T(\mathbf{U}_h - \mathbf{U}_h^H)}_{\text{error in computable correction}}\end{aligned} \tag{12}$$

where $\mathbf{R}_h$ is the solution residual computed on the fine mesh. As described by Pierce and Giles,[49] to effectively reduce the functional error, both the primal and adjoint residuals need to be reduced. Two formulations of an error indicator for mesh adaptation can be obtained from Equation (12). Firstly, the so-called computable correction (CC) given by

$$\varepsilon_{K_H} = \sum_{l(k)} \left\{ \left| \left[(\mathbf{\Psi}_h^H)^T \mathbf{R}_h(\mathbf{U}_h^H) \right]_{l(k)} \right| \right\} \tag{13}$$

where ε_{K_H} is summed over the fine spaces $l(k)$ and secondly, the error in the computable correction (ECC) as described by Becker and Rannacher[29] and Venditti and Darmofal[32,33,48] which replaces Equation (13) with the next-order contributions of the primal residual error weighted by the adjoint and adjoint residual error weighted by the primal solution. Venditti and Darmofal[32,33,48] proposed a form of the error indicator based on the ECC which can be expressed as

$$\varepsilon_{K_H} = \sum_{l(k)} \left\{ \frac{1}{2} \left| \left[\mathbf{Q}_h^H \mathbf{\Psi}_H - \mathbf{L}_h^H \mathbf{\Psi}_H \right]_{l(k)}^T \left[\mathbf{R}_h(\mathbf{L}_h^H \mathbf{U}_H) \right]_{l(k)} \right| + \frac{1}{2} \left| \left[\mathbf{Q}_h^H \mathbf{U}_H - \mathbf{L}_h^H \mathbf{U}_H \right]_{l(k)}^T \left[\mathbf{R}_h^\Psi(\mathbf{L}_h^H \mathbf{\Psi}_H) \right]_{l(k)} \right| \right\} \tag{14}$$

where $\mathbf{R}_h^\Psi$ represents the residual of the discrete adjoint equations, $\mathbf{U}_H$, $\mathbf{\Psi}_H$ refer to the coarse space primal and adjoint solutions, respectively, and $\mathbf{Q}_h^H$ and $\mathbf{L}_h^H$ are quadratic and linear interpolators, respectively, for transferring the solution from the coarse to fine spaces (See Barth[50]). Since the ECC form of the error indicator incorporates a measure of the adjoint residual (unlike the computable correction formulation), it facilitates a more consistent reduction in the functional error estimate, thereby increasing the functional accuracy when used as a driver for anisotropic AMR.

IV.B. Calculation of Fine-Space Error Indicator via p-Refinement

An alternative approach to the evaluation of the fine-space error indicator is also considered here based on a p-refinement strategy wherein the high-order CENO finite-volume scheme described above is used to evaluate the residual to higher spatial accuracy. This alternative procedure follows other similar strategies proposed previously by Yano and Darmofal,[51] Ceze and Fidkowski,[39] and Woopen *et al.*[52] In this case, the initial coarse space primal solution, $\mathbf{U}_{H,P}$, and functional, $J_{H,P}(\mathbf{U}_{H,P})$, are evaluated on the coarse mesh using the limited second-order ($P = 2$) finite-volume scheme, where P represents the order of the spatial discretization scheme. The corresponding fine space estimates of these quantities are $\mathbf{U}_{H,p}^P$, and $J_{H,p}(\mathbf{U}_{H,p}^P)$, respectively, for $p > P$. In this case, the error indicator based on the computable correction becomes

$$\varepsilon_{K_{H,P}} = \left| (\mathbf{\Psi}_{H,p}^P)^T \mathbf{R}_{H,p}(\mathbf{U}_{H,p}^P) \right| \tag{15}$$

and the corresponding expression for the ECC-based error indicator is then

$$\varepsilon_{K_{H,P}} = \frac{1}{2} \left| \left[\mathbf{\Psi}_{H,p}^P - \mathbf{\Psi}_{H,P} \right] \left[\mathbf{R}_{H,p}(\mathbf{U}_{H,p}^P) \right] \right| + \frac{1}{2} \left| \left[\mathbf{U}_{H,p}^P - \mathbf{U}_{H,P} \right] \left[\mathbf{R}_{H,p}^\Psi(\mathbf{\Psi}_{H,p}^P) \right] \right| \tag{16}$$

where $\mathbf{U}_{H,P}$ and $\mathbf{\Psi}_{H,P}$ are the coarse space primal and adjoint solutions, $\mathbf{R}_{H,p}(\mathbf{U}_{H,p}^P)$ and $\mathbf{R}_{H,p}^\Psi(\mathbf{\Psi}_{H,p}^P)$ are the higher-order or fine-space estimates of the solution residual and adjoint residual respectively, $\mathbf{U}_{H,p}^P$ is a

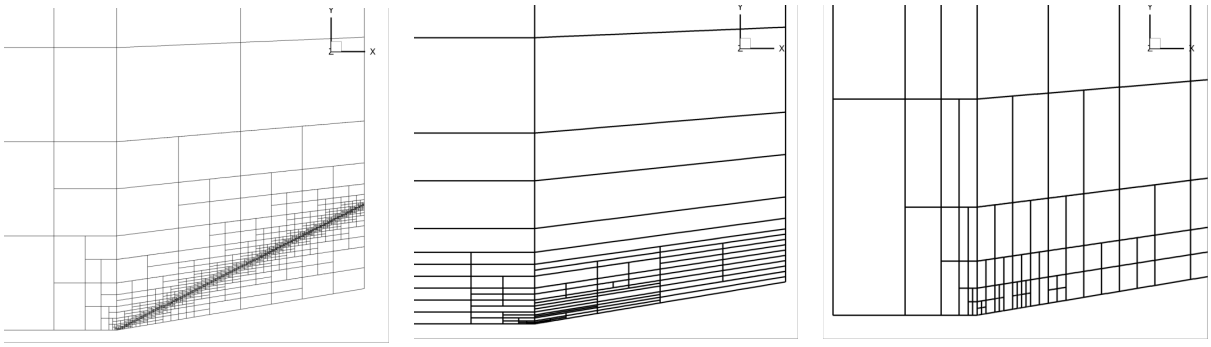

(a) Close-up of final mesh utilizing gradient based AMR, 9 levels of AMR, 1523 blocks (3,119,104 cells).

(b) Close-up of final mesh utilizing output-based AMR (h-derived ECC error indicator). 12 levels of AMR, 115 blocks (111,760 cells), resulting in up to 97% mesh savings when compared to the gradient-based AMR mesh.

(c) Close-up of final mesh using output-based AMR (p-derived ECC error indicator). 7 levels of AMR, 197 blocks (201,728 cells), resulting in up to 53% mesh savings when compared to the gradient-based AMR mesh.

Figure 3: Final adapted meshes obtained via gradient- and output-based AMR results for supersonic flow (M=3.0) over a wedge. The output-based approach led to significant cell count savings.

higher p-order reconstruction of coarse polynomial space $\mathbf{U}_{H,P}$, $\mathbf{\Psi}^P_{H,p}$ is a p-order reconstruction of coarse space $\mathbf{\Psi}_{H,P}$. For this study to date, the coarse space ($\Omega_{H,P}$) was second-order accurate, and the fine space, ($\Omega_{H,p}$) was based on the third-order accurate CENO scheme with $p = 3$.

IV.C. Criteria for Anisotropic Mesh Refinement

In order to allow for anisotropic refinement with the h-refinement approach described above, three different coarse spaces are created by refining the mesh preferentially in each of the logical coordinate directions associated with the mesh blocks of the multi-block body fitted mesh. A set of three directional dependent error indicators are then calculated and then used to drive the mesh refinement in the preferred directions that results in lower values of the error in the functional. Anisotropic refinement with the preceding p-refinement approach is accomplished by utilizing the anisotropic smoothness indicator as proposed by Freret *et al.*[27] and given in Equations (10)-(11). Once the isotropic p-space error indicators are evaluated to identify relevant blocks for refinement (or coarsening), the smoothness of the density solution variable is evaluated using the anisotropic smoothness indicator. The logical coordinate direction having the largest measure of non-smoothness determines the preferred direction for refinement.

V. Numerical Results for Inviscid Flows

Numerical results obtained using the proposed output-based anisotropic AMR scheme are now considered for several steady inviscid compressible flow problems. In particular, results are discussed for steady inviscid supersonic flow past a wedge, steady inviscid subsonic flow over a smooth bump in a channel, and steady inviscid transonic flow past an airfoil. Results in terms of accuracy and computational cost (time and storage requirements) will be compared for the grids refined via output-based methods, using, as a baseline, results obtained via gradient-based AMR and uniform refinement. For all these approaches, the quantity of interest to be calculated will be the pressure drag on selected geometry surfaces, and this will be utilized to compare the accuracy of these approaches for various flow regimes. The output-based AMR approach will utilize the evaluation of the adjoint and use this to weight the solution residual, thereby calculating an error indicator which marks regions with the largest error for mesh refinement. The gradient-based approach will mark regions for refinement based on the rates of change of density. Uniform refinement does not perform selective refinement; the entire mesh is refined. In the following set of results, the h-derived error indicator based on the error in the computable correction is referred to as h-ECC, while the corresponding error indicator based on the computable correction is h-CC. For the error indicators based on the error in the

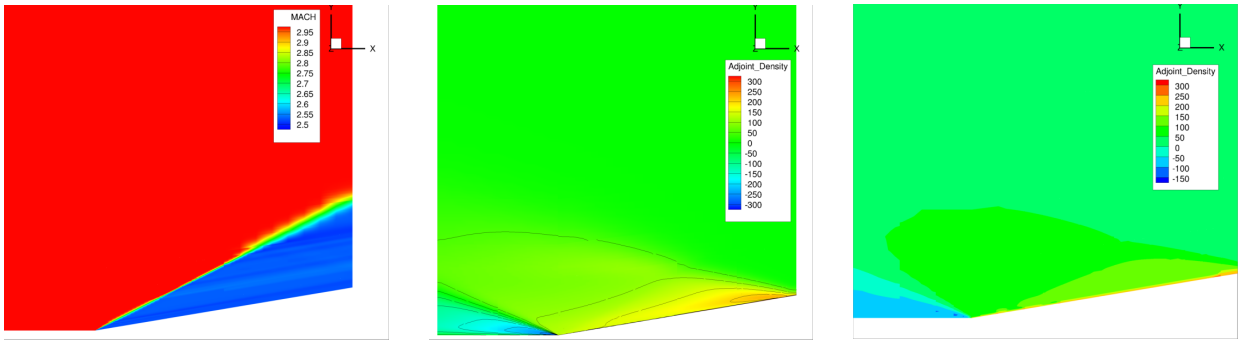

(a) Contours of Mach Number on mesh in Figure 3c adapted via $p-$derived error estimates based on the ECC.

(b) Contours of density adjoint on mesh in Figure 3b adapted via $h-$derived error estimates based on the ECC.

(c) Contours of density adjoint on mesh in Figure 3c adapted via $p-$derived error estimates based on the ECC.

Figure 4: Contours of Mach number and density adjoint for supersonic flow (M=3.0) over a wedge on meshes adapted via output-based AMR.

computable correction and the computable correction based on the p-derived approach are referred to as the p-ECC and p-CC error indicators respectively.

V.A. Steady Supersonic Inviscid Flow Past a Wedge

Numerical results are first considered for steady inviscid supersonic flow over a wedge similar to that carried out by Hartmann and Houston,[53] with a flow Mach number of 3.0. The wedge angle was set at 9.5° with a total wedge surface dimension of 0.986 m length, and 0.25 m depth. The analytic value of the pressure drag on the wedge surface was calculated to be 8308.27 N. The gradient-based approach utilized density gradient as the refinement criteria, while for the adjoint-based approach, the functional of interest was taken to be the pressure drag on the surface of the wedge.

The functional accuracy versus mesh size for gradient-based and adjoint-based error estimates based on both the h- and p-refinement approaches were obtained and compared. The gradient of the density was used as criteria for the gradient-based approach. To compare the output-based AMR results, the gradient-based refinement AMR results and those obtained via uniform refinement were considered as a baseline result. For

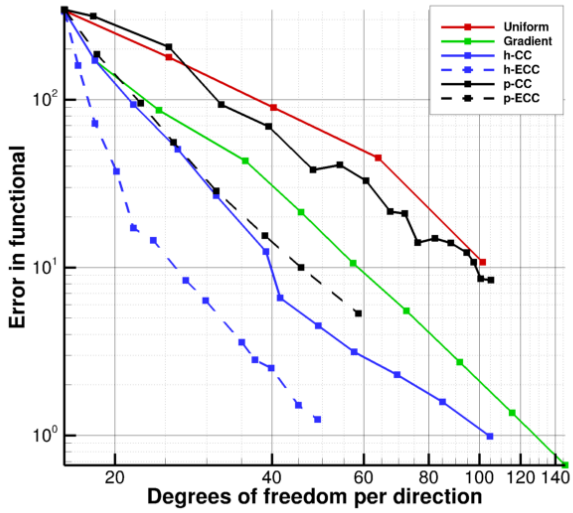

Figure 5: Convergence plot of functional accuracy versus mesh size for supersonic flow (M=3.0) over a wedge.

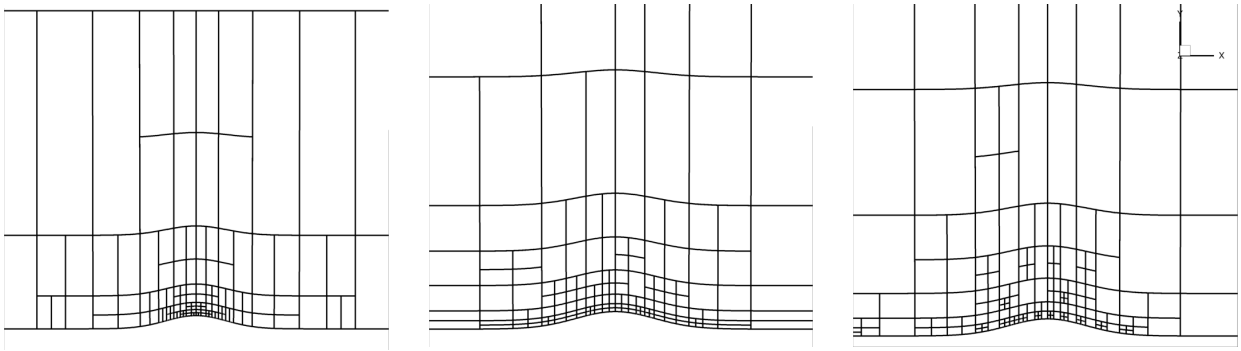

(a) Close-up showing final mesh with gradient-based AMR, 4 levels of AMR, 130 blocks (133,120 cells).

(b) Close-up showing final mesh adapted via output-based h-derived ECC. 7 AMR levels, 304 blocks (311,296 cells).

(c) Close-up showing final mesh adapted via output-based p-derived ECC. 6 AMR levels, 343 blocks (351,232 cells).

Figure 6: Final meshes for subsonic flow (M = 0.1) over a Gaussian bump obtained using gradient- and adjoint-based AMR.

the adjoint-based methods, error indicators were based on the computable correction (CC) and the Venditti-Darmofal formulation of the error indicator based on the error in the computable correction (ECC). The final refined meshes for both the gradient-based and adjoint-based AMR strategies are shown in Figure 3. It can be observed that the adapted mesh of the gradient-based approach as shown in Figure 3a has the highest resolution in the vicinity of the shock, whereas the adjoint-based methods produce meshes which are adapted primarily in the vicinity of the leading edge of the wedge. The adjoint depicts sensitivity to perturbations in regions lying upstream of the geometrical surface changes for the wedge, at approximately the wedge angle (9.5°), as seen in Figures 4b and 4c.

The convergence of the functional error (pressure drag on the wedge surface) as a function of mesh density for the various refinement strategies is given in Figure 5. From this, it is observed that the adjoint-based approach, particularly, the ECC formulation, would seem to provide the most effective refinement of the mesh, (up to 97% savings), leading to adapted meshes with the most accurate computed functional for the same mesh density. Although the uniform approach obviously leads to an accurate functional as shown in Figure 5, the resulting mesh size would be very large as compared to those obtained using AMR, in particular, those achieved with the output-based AMR strategies. It is also worth noting that it was found that the evaluation of the p-refinement based error indicator based on the high-order CENO scheme residual required up to about 4-5 times less computational effort than the corresponding evaluation of h-refinement based error indicator. The computational and memory requirements of the various strategies will be explored in greater in follow-on studies.

V.B. Steady Inviscid Subsonic Flow Over a Bump in a Channel

Next, numerical results are considered for steady inviscid subsonic flow over a Gaussian bump, at a Mach number of 0.1. The channel has dimensions 3 m length, 0.8 m height and 1 m depth. The profile of the bump is given by $y = 0.0625e^{-25x^2}$. The pressure drag acting on the bump was taken as the function of interest. The final adapted meshes for both the gradient-based and adjoint-based AMR strategies are shown in Figure 6a, Figure 6b and Figure 6c. The spatial rate of change of the density was used as mesh refinement criteria for the gradient-based approach. For the adjoint-based methods, error indicators were based on both the CC and the ECC formulations. The predicted distribution of adjoint for this problem exhibits variations in regions of the computational domain corresponding to the largest density variation adjacent to the bump surface as shown in Figures7b and 7c.

Convergence of the estimated error in the computed functional as a function of mesh density for the various refinement strategies is depicted in Figure 8. Interestingly, the numerical results indicate that the effectiveness of the simple gradient-based AMR is at least comparable if not somewhat superior to that of the output-based approaches for this case. This may not be too surprising as this low-Mach-number flow as possesses a very smooth and regular solution for which the regions of high solution gradients would be

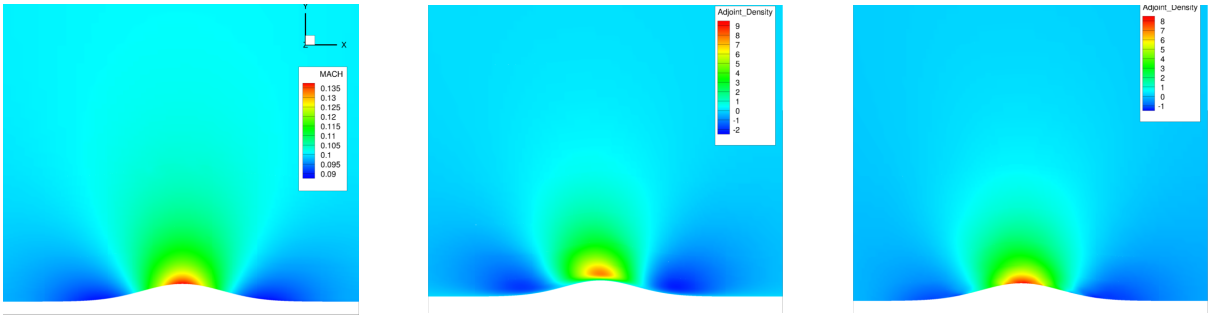

(a) Close-up showing Mach number contours on output-based AMR mesh shown in Figure 6c obtained via p-derived output-based error indicators.

(b) Close-up showing contours of density adjoint on output-based AMR mesh shown in Figure 6b obtained via h-derived output-based error indicators.

(c) Close-up showing contours of density adjoint on output-based AMR mesh shown in Figure 6c obtained via p-derived output-based error indicators.

Figure 7: Contours of Mach number and density adjoint for supersonic flow (M=0.1) over a Gaussian bump in a channel on meshes adapted via output-based AMR.

expected to correlate well the error. Nevertheless, as for the supersonic wedge flow, the performance of all of the AMR strategies considerably outperforms the uniform mesh refinement approach, requiring significantly larger meshes for the same accuracy. In comparing the performances of the ECC and the CC formulations of the error indicator for directing the output-based AMR for this case, it can be seen that both methods yielded similar estimates of the functional accuracies with neither being more preferential by a significant margin. As for the previous wedge flow, it was found that the evaluation of the p-based indicators required only about 4-5 times the computational cost of the corresponding evaluation of h-refinement based error indicator while providing similar performance in terms of refinement efficiency and accuracy, which is rather significant.

V.C. Steady Inviscid Transonic Flow Past a NACA 0012 Airfoil

Finally, numerical results for steady inviscid transonic flow at Mach 0.8 over a NACA 0012 airfoil, represented in a C-grid type mesh, of 1 m chord length at an angle of attack of 1.25° were investigated. The functional

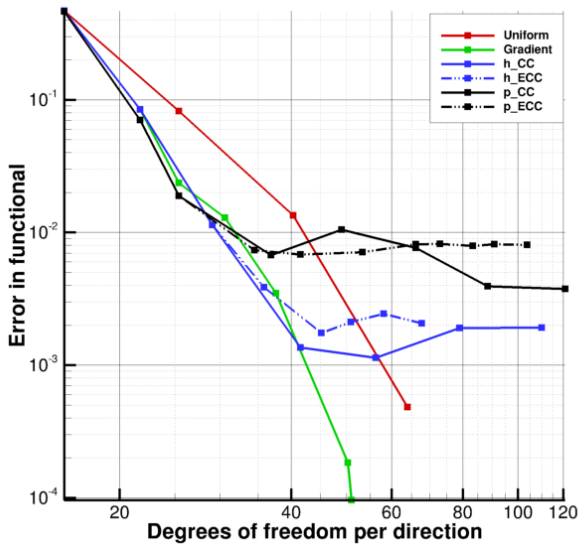

Figure 8: Convergence plot of functional accuracy versus mesh size for subsonic flow (M = 0.1) over a Gaussian bump.

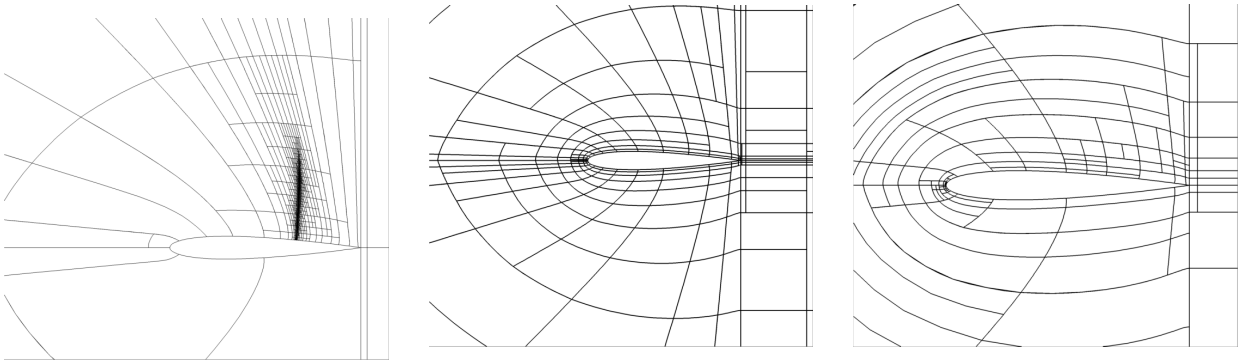

(a) Close-up showing final gradient-based mesh after 12 levels of AMR, 1945 blocks (1,991,680 cells).

(b) Close-up showing final output-based AMR mesh after 4 levels of AMR refined via h-derived ECC error indicator, 285 blocks (= 291,840 cells), representing 85% cell count savings when compared to the gradient-based AMR mesh.

(c) Close-up showing final output-based AMR mesh after 8 levels of AMR refined via p-derived ECC error indicator, 334 blocks (= 342,016 cells), representing 72% cell count savings when compared to the gradient-based AMR mesh.

Figure 9: Final meshes for gradient- and output-based AMR results for transonic flow over a NACA 0012 airfoil.

was again taken to be the pressure drag, and convergence of the drag coefficient, C_d was monitored. The functional accuracy versus mesh size for gradient-based and output-based error estimates based on both the h- and p-refinement approaches were obtained and compared. The density gradient was used as mesh refinement criteria for the gradient-based AMR. For the output-based methods, error indicators were based on the CC and the ECC.

The final refined meshes for both the gradient-based and output-based AMR strategies are shown in Figure 9. The gradient-based mesh adaptation strategy clearly focuses the mesh resolution in the vicinity of the shock that forms on the upper wing surface where the gradients are very large, while the output-based approach results in a mesh that has the highest resolution around the leading edge stagnation point, as well as at the trailing edge. While the shock is identified by the gradient-based method as a region for refinement, the pressure drag on the airfoil surface is not dependent on the accuracy of the solution of this

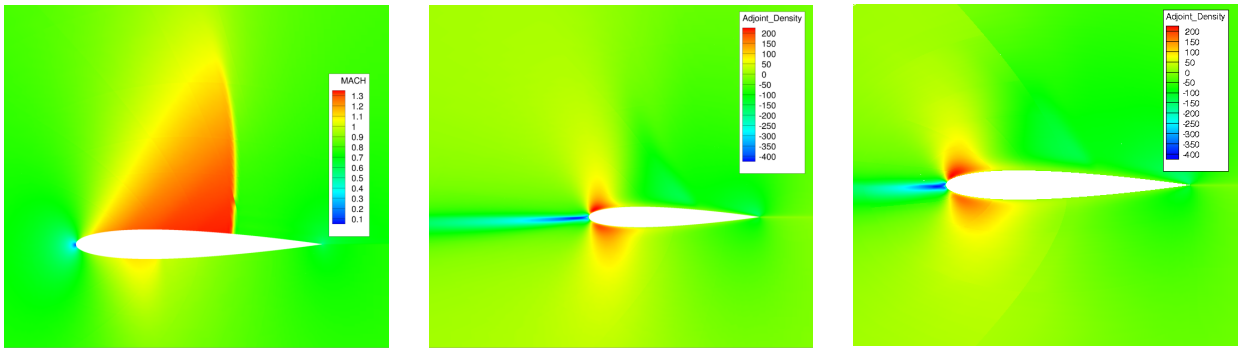

(a) Close-up showing Mach number contours on mesh obtained via output-based p-derived ECC error indicator for AMR shown in Figure 9c.

(b) Close-up showing density adjoint contours on mesh obtained via output-based h-derived ECC error indicator for AMR shown in Figure 9b.

(c) Close-up showing density adjoint contours on mesh obtained via output-based p-derived ECC error indicator for AMR shown in Figure 9c.

Figure 10: Mach number and density adjoint contours for transonic flow (M = 0.8) over a NACA0012 Airfoil at an angle of attack of 1.25°.

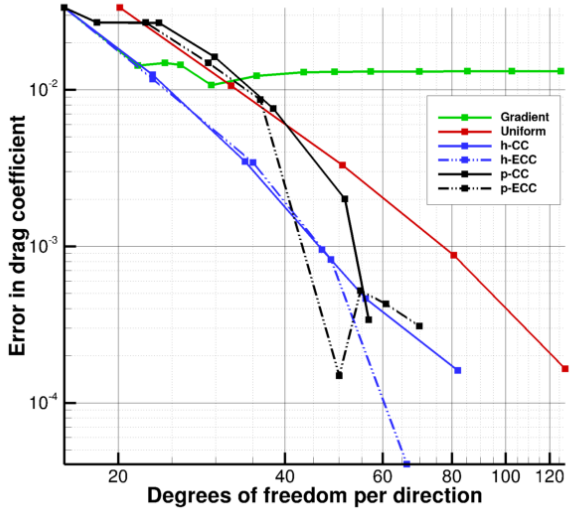

Figure 11: Convergence plot of functional accuracy versus mesh size for transonic flow (M = 0.8) over a NACA 0012 airfoil.

region and hence the mesh enrichment there is wasted. Conversely, the predicted distribution of the adjoint captures the high sensitivity of the functional to errors in the primal solutions in a region just upstream and downstream of the leading edge stagnation point near the leading edge of the airfoil as depicted in Figure 10. This leads to enhance resolution near the leading edge as the mesh is refined and a correspondingly more accurate estimate of the pressure drag.

The convergence of the estimated error in the functional versus the mesh density for the various refinement strategies is given in Figure 11 for the NACA 0012 airfoil case. The results show that the output-based AMR approach, particularly the ECC formulation, led to the most accurate and efficient evaluation of the functional. As with the other two cases described above, the computational effort associated with the evaluation of the p-based refinement indicators were found to be considerably less than those associated with the evaluation of the h-based indicators.

VI. Conclusions

A number of representative solutions to inviscid compressible flows governed by the Euler equations have been considered. An output-based error estimation strategy has been developed and combined with an efficient and highly scalable parallel anisotropic block-based AMR technique for the prediction of inviscid compressible three-dimensional inviscid flows. The evaluation of error indicators for the target function based on both h- and p-refinement procedures has been considered and the computational efficiencies associated with the p-refinement approach have been identified. The output-based error estimation for directing the AMR was found to offer performance benefits when compared to physics-based methods, particularly in the presence of discontinuities and sharp gradients. In majority of the flow problems considered, particularly those with sharp solution gradients, the output-based methods led to the most accurate functional for the smallest mesh size in comparison to the reference gradient-based AMR and uniform refinement approaches. For the supersonic wedge flow case, the gradient-based AMR strategy yielded the largest mesh sizes with relatively lowest accuracy and, for the transonic NACA0012 airfoil flow, the gradient-based directed AMR method failed to produce a converged estimate of the functional. Of the output-based approaches, the Venditti-Darmofal formulation of the ECC-based error indicator led to the most accurate calculations of the functional for the wedge and airfoil cases. Additionally, the adaptation method based on the h-derived error estimates provided the more accurate calculations of the functionals, as compared to corresponding those of the p-refinement based strategy. Nevertheless, the latter was found to perform well and incurred considerably less computational cost. For the p-derived error indicator, the proposed anisotropic smoothness indicator was shown to identify successfully the appropriate directional bias for mesh refinement. As may be expected, the output-based approaches did not offer considerably higher functional accuracy for reduced mesh sizes

for the smooth inviscid subsonic flow case considered. Follow-on research will consider the application of the combined output-based error estimation and anisotropic AMR schemes to three-dimensional compressible viscous flows.

Acknowledgments

This work was supported by the Canadian Space Agency and by the Natural Sciences and Engineering Research Council (NSERC) of Canada. In particular, the authors would like to acknowledge the financial support received from the Canadian Space Agency through the Geospace Observatory Canada program. Computational resources for performing all of the calculations reported herein were provided by the SciNet High Performance Computing Consortium at the University of Toronto and Compute/Calcul Canada through funding from the Canada Foundation for Innovation (CFI) and the Province of Ontario, Canada.

References

[1]Berger, M. J., *Adaptive Mesh Refinement for Hyperbolic Partial Differential Equations*, Ph.D. thesis, Stanford University, January 1982.

[2]Berger, M. J. and Oliger, J., "Adaptive Mesh Refinement for Hyperbolic Partial Differential Equations," *J. Comput. Phys.*, Vol. 53, 1984, pp. 484–512.

[3]Berger, M. J., "Data Structures for Adaptive Grid Generation," *SIAM J. Sci. Stat. Comput.*, Vol. 7, No. 3, 1986, pp. 904–916.

[4]Berger, M. J. and Colella, P., "Local Adaptive Mesh Refinement for Shock Hydrodynamics," *J. Comput. Phys.*, Vol. 82, 1989, pp. 64–84.

[5]Berger, M. J. and Saltzman, J. S., "AMR on the CM-2," *Appl. Numer. Math.*, Vol. 14, 1994, pp. 239–253.

[6]Groth, C. P. T., De Zeeuw, D. L., Powell, K. G., Gombosi, T. I., and Stout, Q. F., "A Parallel Solution-Adaptive Scheme for Ideal Magnetohydrodynamics," Paper 99-3273, AIAA, June 1999.

[7]Groth, C. P. T., De Zeeuw, D. L., Gombosi, T. I., and Powell, K. G., "Three-Dimensional MHD Simulation of Coronal Mass Ejections," *Adv. Space Res.*, Vol. 26, No. 5, 2000, pp. 793–800.

[8]Aftosmis, M. J., Berger, M. J., and Adomavicius, G., "A Parallel Multilevel Method for Adaptively Refined Cartesian Grids with Embedded Boundaries," Paper 2000-0808, AIAA, January 2000.

[9]Gao, X. and Groth, C. P. T., "A Parallel Solution-Adaptive Method for Three-Dimensional Turbulent Non-Premixed Combusting Flows," *J. Comput. Phys.*, Vol. 229, No. 5, 2010, pp. 3250–3275.

[10]Northrup, S. A., *A Parallel Implicit Adaptive Mesh Refinement Algorithm for Predicting Unsteady Fully-Compressible Reactive Flows*, Ph.D. thesis, University of Toronto, December 2013.

[11]Charest, M. R. J., Groth, C. P. T., and Gülder, Ö. L., "Numerical Study on the Effect of Gravity on Flame Shape and Radiation in Laminar Diffusion Flames," *Proceedings of the Combustion Institute Canadian Section Spring Technical Meeting*, Toronto, Canada, May 12–14 2008, pp. 84–89.

[12]Gao, X. and Groth, C. P. T., "Parallel Adaptive Mesh Refinement Scheme for Three-Dimensional Turbulent Non-Premixed Combustion," Paper 2008-1017, AIAA, January 2008.

[13]Gao, X., *A Parallel Solution-Adaptive Method for Turbulent Non-Premixed Combusting Flows*, Ph.D. thesis, University of Toronto, August 2008.

[14]Charest, M. R. J. and Groth, C. P. T., "A High-Order Central ENO Finite-Volume Scheme for Three-Dimensional Turbulent Reactive Flows on Unstructured Mesh," Paper 2013-2567, AIAA, June 2013.

[15]Freret, L. and Groth, C. P. T., "Anisotropic Non-Uniform Block-Based Adaptive Mesh Refinement for Three-Dimensional Inviscid and Viscous Flows," Paper 2015-2613, AIAA, June 2015.

[16]Northrup, S. A. and Groth, C. P. T., "Parallel Implicit Adaptive Mesh Refinement Scheme for Unsteady Fully-Compressible Reactive Flows," Paper 2013-2433, AIAA, June 2013.

[17]Northrup, S. A. and Groth, C. P. T., "Solution of Laminar Diffusion Flames Using a Parallel Adaptive Mesh Refinement Algorithm," Paper 2005–0547, AIAA, January 2005.

[18]Gao, X., Northrup, S. A., and Groth, C. P. T., "Parallel Solution-Adaptive Method for Two-Dimensional Non-Premixed Combusting Flows," *Prog. Comput. Fluid Dyn.*, Vol. 11, No. 2, 2011, pp. 76–95.

[19]Gao, X. and Groth, C. P. T., "Parallel Adaptive Mesh Refinement Scheme for Turbulent Non-Premixed Combusting Flow Prediction," Paper 2006-1448, AIAA, January 2006.

[20]Gao, X. and Groth, C. P. T., "A Parallel Adaptive Mesh Refinement Algorithm for Predicting Turbulent Non-Premixed Combusting Flows," *Int. J. Comput. Fluid Dyn.*, Vol. 20, No. 5, 2006, pp. 349–357.

[21]Jha, P. K., *Modelling Detailed-Chemistry Effects on Turbulent Diffusion Flames Using a Parallel Solution-Adaptive Scheme*, Ph.D. thesis, University of Toronto, October 2011.

[22]Ivan, L., De Sterck, H., Northrup, S. A., and Groth, C. P. T., "Three-Dimensional MHD on Cubed-Sphere Grids: Parallel Solution-Adaptive Simulation Framework," Paper 2011-3382, AIAA, June 2011.

[23]Ivan, L., De Sterck, H., Northrup, S. A., and Groth, C. P. T., "Hyperbolic Conservation Laws on Three-Dimensional Cubed-Sphere Grids: A Parallel Solution-Adaptive Simulation Framework," *J. Comput. Phys.*, Vol. 255, 2013, pp. 205–227.

[24]Susanto, A., Ivan, L., Sterck, H. D., and Groth, C. P. T., "High-Order Central ENO Finite-Volume Scheme for Ideal MHD," *J. Comput. Phys.*, Vol. 250, 2013, pp. 141–164.

[25]Zhang, Z. J. and Groth, C. P. T., "Parallel High-Order Anisotropic Block-Based Adaptive Mesh Refinement Finite-Volume Scheme," Paper 2011-3695, AIAA, June 2011.

[26]Williamschen, M. J. and Groth, C. P. T., "Parallel Anisotropic Block-Based Adaptive Mesh Refinement Algorithm For Three-Dimensional Flows," Paper 2013-2442, AIAA, June 2013.

[27]Freret, L., Ivan, L., De Sterck, H., and Groth, C. P. T., "A High-Order Finite-Volume Method with Anisotropic AMR for Ideal MHD Flows," Paper 2017-0845, AIAA, January 2017.

[28]Giles, M. B. and Pierce, N. A., "An Introduction to the Adjoint Approach to Design," *Flow Turb. Combust.*, Vol. 65, 2000, pp. 393–415.

[29]Becker, R. and Rannacher, R., "An Optimal Control Approach to A Posteriori Error Estimation in Finite Element Methods," *Acta Num.*, Vol. 10, 2001, pp. 1–102.

[30]Becker, R., Heuveline, V., and Rannacher, R., "An Optimal Control Approach to Adaptivity in Computational fluid Dynamics," *Int. J. Numer. Meth. Fluids*, Vol. 40, 2002, pp. 105–120.

[31]Heuveline, V. and Rannacher, R., "Duality-Based Adaptivity in the *hp*-Finite Element Method," *J. Numer. Math.*, Vol. 11, 2003, pp. 95–103.

[32]Venditti, D. A. and Darmofal, D. L., "Adjoint Error Estimation and Grid Adaptation for Functional Outputs: Application to Quasi-One-Dimensional Flow," *J. Comput. Phys.*, Vol. 164, 2000, pp. 204– 227.

[33]Venditti, D. A. and Darmofal, D. L., "Grid Adaptation for Functional Outputs: Application to Two-Dimensional Inviscid Flows," *J. Comput. Phys.*, Vol. 176, 2002, pp. 40– 69.

[34]Venditti, D. A. and Darmofal, D. L., "Anisotropic Grid Adaptation for Functional Outputs: Application to Two-Dimensional Viscous Flows," *J. Comput. Phys.*, Vol. 187, 2003, pp. 22– 46.

[35]Rannacher, R. and Vexler, B., "A Priori Error Estimates for the Finite Element Discretization of Elliptic Parameter Identification Problems with Pointwise Measurements," *SIAM J. Control Opt.*, Vol. 44, 2005, pp. 1844–1863.

[36]Nemec, M. and Aftosmis, M. J., "Adjoint Error Estimation and Adaptive Refinement for Embedded-Boundary Cartesian Meshes," Paper 2007-4187, AIAA, June 2007.

[37]Nemec, M. and Aftosmis, M. J., "Adjoint Sensitivity Computations for an Embedded-Boundary Cartesian Mesh Method," *J. Comput. Phys.*, Vol. 227, No. 4, 2008, pp. 2724–2742.

[38]Ceze, M. A. and Fidkowski, K. J., "A Robust Adaptive Solution Strategy for High-Order Implicit CFD Solvers," Paper 2011-3696, AIAA, 2011.

[39]Ceze, M. A. and Fidkowski, K. J., "An Anisotropic *hp*-Adaptation Framework for Functional Prediction," *AIAA J.*, Vol. 51, No. 2, 2013, pp. 492–509.

[40]Ivan, L. and Groth, C. P. T., "High-Order Solution-Adaptive Central Essentially Non-Oscillatory (CENO) Method for Viscous Flows," *J. Comput. Phys.*, Vol. 257, 2014, pp. 830–862.

[41]Toro, E. F., *Riemann Solvers and Numerical Methods for Fluid Dynamics: A Practical Introduction*, Springer-Verlag, New York, 1999.

[42]Einfeldt, B., "On Godunov-Type Methods for Gas Dynamics," *SIAM J. Numer. Anal.*, Vol. 25, 1988, pp. 294–318.

[43]Saad, Y. and Schultz, M. H., "GMRES: A Generalized Minimal Residual Algorithm for Solving Nonsymmetric Linear Equations," *SIAM J. Sci. Stat. Comput.*, Vol. 7, No. 3, 1986, pp. 856–869.

[44]Gropp, W., Lusk, E., and Skjellum, A., *Using MPI*, MIT Press, Cambridge, Massachussets, 1999.

[45]Gropp, W., Lusk, E., and Thakur, R., *Using MPI-2*, MIT Press, Cambridge, Massachussets, 1999.

[46]Harten, A., Enquist, B., Osher, S., and Chakravarthy, S. R., "Uniformly High Order Accurate Essentially Non-Oscillatory Schemes, III," Report 86-22, ICASE, April 1986.

[47]Jiang, G.-S. and Shu, C.-W., "Efficient Implementation of Weighted ENO Schemes," *J. Comput. Phys.*, Vol. 126, 1996, pp. 202–228.

[48]Venditti, D. A. and Darmofal, D. L., "Anisotropic Adaptation for Functional Outputs of Viscous Flow Simulations," Paper 2003-3845, AIAA, June 2003.

[49]Pierce, N. A. and Giles, M. B., "Adjoint Recovery of Superconvergent Functionals from PDE Approximations," *SIAM Rev.*, Vol. 42, No. 2, 2000, pp. 247–264.

[50]Barth, T. J. and Fredrickson, P. O., "Higher Order Solution of the Euler Equations on Unstructured Grids Using Quadratic Reconstruction," Paper 90-0013, AIAA, January 1990.

[51]Yano, M. and Darmofal, D. L., "An Optimization Framework for Anisotropic Simplex Mesh Adaptation," *J. Comput. Phys.*, Vol. 231, 2012, pp. 7626–7649.

[52]Woopen, M., Balan, A., May, G., and Schütz, J., "A Comparison of Hybridized and Standard DG Methods for Target-Based *hp*-Adaptive Simulation of Compressible Flow," *Comp. Fluids*, Vol. 98, 2014, pp. 3–16.

[53]Hartmann, R. and Houston, P., "Error Estimation and Adaptive Mesh refinement for Aerodynamic Flows," *von Karman Institute for Fluid Dynamics Lecture Series 2010-01, 36th CFD/ADIGMA Course on* hp-*Adaptive and* hp-*Multigrid Methods, October 26–30, 2009*, von Karman Institute for Fluid Dynamics, Rhode Saint Genese, Belgium, 2009.